© 2014. Published by The Company of Biologists Ltd | The Journal of Experimental Biology (2014) 217, 2277-2287 doi:10.1242/jeb.101949

RESEARCH ARTICLE

Magnetic resonance imaging analysis of water flow in the mantle cavity of live *Mytilus galloprovincialis*

Eriko Seo[1], Kazue Ohishi[2], Tadashi Maruyama[2], Yoshie Imaizumi-Ohashi[3], Masataka Murakami[4] and Yoshiteru Seo[3,*]

ABSTRACT

Water flow inside the shell of *Mytilus galloprovincialis* was measured by phase-contrast magnetic resonance imaging (MRI). In seawater without algal cells at 23°C, water approached the mussel from the posterior-ventral side, and entered through the inhalant aperture at a velocity of 40–20 mm s^{-1}. The flow rate in the lower mantle cavity decreased to 10–20 mm s^{-1}, the water flowed in the anterior–dorsal direction and approached the demibranches at a velocity of 5–10 mm s^{-1}. After passing through the lamellae to the upper mantle cavity, the water stretched the interlamellar cavity, turned to the posterior–dorsal direction and accumulated in the epibranchial cavity. The water flows came together at the ventral side of the posterior adductor muscle. The velocity increased more to than 50 mm s^{-1} in the exhalant siphon, and exhaled out in the posterior–dorsal direction. The anterior–posterior direction of the flow was imaged every 1.92 s by the inflow effect of T_1-weighted MRI. The flow seemed to be constant, and no cyclic motion of the mantles or the gills was detected. Spontaneous closure of the shells caused a quick drop of the flow in the mantle cavity. In the opening process of the shells, water flow in the interlamellar cavities increased before the opening, followed by an increase of flows in the exhalant siphon and inhalant aperture with minimum delay, reaching a plateau within 1 min of the shells opening. This provides direct evidence that the lateral cilia drive water in the mussel *M. galloprovincialis*.

KEY WORDS: Mussel pump, Ventilation, Lateral cilia, Filter-feeding bivalve, MRI

INTRODUCTION

Mussels and other filter-feeding bivalves uptake a large amount of water from the inhalant aperture. The suspended particles are then filtered by the gill, and the water leaves from the exhalant siphon (Wallengren, 1905; Mill, 1972; Jørgensen et al., 1986a). Intensive studies have been conducted to measure the filtration rate, using either particle clearance or direct measurements of inhalant and exhalant flows (Bayne, 1976; Kiøboe et al., 1980; Riisgård, 2001). The exhalant jet velocity of mussels has been reported in a range of 80–30 mm s^{-1} for *Mytilus* (Maire et al., 2007; MacDonald et al., 2009; Riisgård et al., 2011). The introduction of video endoscopy (Ward et al., 1991) has made it possible to conduct *in vivo* observation of the gills inside the shell, and also to estimate the water flow from movement of microspheres in the seawater. In the filibranchs and eulamellibranchs, the respiratory flow of water is produced solely by the lateral cilia on the gill filaments (Mill, 1972). There have been numerous studies on the function of the lateral cilia (Bayne, 1976; Beninger and Le Pennec, 2006), and water motion and particle capture in the gill of mussels have been studied intensively (Nielsen et al., 1993; Riisgård et al., 1996). The fluid mechanics of the lateral cilia have also been studied extensively, with some studies focusing on the isolated gill filaments (Jørgensen, 1982; Jørgensen et al., 1986b; Jørgensen et al., 1988) and some using *in vivo* using video endoscopes (Ward et al., 1998) and horizontal dissecting microscopes (Riisgård and Larsen, 2000). However, there is a lack of knowledge regarding volume flow in the mantle cavity. For example, the patterns of flow through the mantle cavity of the mussel are presumably less well defined, and it is necessary to assume a cross-sectional area and length for the mantle cavity to analyse the water flow (Jørgensen et al., 1986a). Indeed, even using a dissecting microscope, water flow is normally estimated by the movement of particles. Until the present study, no one has directly observed the water flow inside the shell of live bivalves.

Magnetic resonance imaging (MRI) is a non-invasive imaging technique, and studies on invertebrates using this technique have been gradually increasing (Bock et al., 2001; Herberholz et al., 2004; Seo et al., 2014). Because the shell consists of non-magnetic solid substances, calcium bicarbonate and conchiolin, it does not interfere with the MRI measurements or raise the magnetic resonance (MR) signal, and so MRI can readily visualize soft tissues and seawater in the shell. In our previous report, we demonstrated that MRI is a precise and non-invasive technique for the measurement of heart rate, estimating the stroke volume of the heart, and determining the flow rate and direction of haemolymph in the heart and adjacent vessels in living *Mytilus galloprovincialis* Lamarck 1819 (Seo et al., 2014). In the present study, we applied phase-contrast MRI in order to determine the flow rate and direction of seawater from the inhalant aperture to the exhalant siphon through the mantle cavity and gills. Then, the patterns of ventilatory flows through the mantle and gills were visualised, and compared with those reported previously as the established classical pattern (Wallengren, 1905; Jørgensen, 1974; Bayne, 1976; Beninger and Le Pennec, 2006). We also measured time-dependent changes in the water flow using T_1-weighted MRI for analysis of quick or spontaneous changes in the flow. In addition, we attempted to confirm that the respiratory flow of water is produced solely by the lateral cilia on the gill filaments, without any contribution of muscular movements of the mantle or gills (Mill, 1972).

[1]Department of Marine Ecosystem Dynamics, Division of Marine Life Science, Atmosphere and Ocean Research Institute, The University of Tokyo, Kashiwa, 277-8564, Japan. [2]Marine Biodiversity Research Program, Institute of Biogeosciences, Japan Agency for Marine-Earth Science and Technology, Yokosuka, 237-0061, Japan. [3]Department of Regulatory Physiology, Dokkyo Medical University School of Medicine, Tochigi, 321-0293, Japan. [4]Department of Molecular Physiology, National Institute for Physiological Sciences, Okazaki, 444-8787, Japan.

*Author for correspondence (yseo@dokkyomed.ac.jp)

Received 30 December 2013; Accepted 14 March 2014

The Journal of Experimental Biology (2014) doi:10.1242/jeb.101949

List of symbols and abbreviations

AV	auriculoventricular
ES	exhalant siphon
FA	flip angle
IA	inhalant aperture
IC	interlamellar connection
ID	inner demibranch
ILCID	interlamellar cavity of inner demibranch
ILCOD	interlamellar cavity of outer demibranch
ILID	inner lamella of inner demibranch
ILOD	inner lamella of outer demibranch
LC	lateral cavity
MC	median cavity
MLC	mediolateral cavity
MR	magnetic resonance
MRI	magnetic resonance imaging
OD	outer demibranch
OLID	outer lamella of inner demibranch
OLOD	outer lamella of outer demibranch
PAM	posterior adductor muscle
PC-MRI	phase-contrast gradient-echo MRI
ROI	region of interest
T_{1w}-MRI	T_1-weighted gradient-echo MRI
T_E	echo time
T_R	relaxation delay

RESULTS

Anatomy of the mantle cavity

The anatomical structure of the mantle cavity of *M. galloprovincialis* is shown in Fig. 1. As no MR signal was detected from the shell, the shell was depicted as black strips between the soft tissues and seawater around the shell (Fig. 1C,D). The mantle cavity is separated into the lower and upper mantle cavities by two pairs of demibranches: the outer and inner demibranches (OD and ID, respectively; Fig. 1A,C). Famme and Kofoed (Famme and Kofoed, 1983) divided the lower mantle cavity into five cavities: a median cavity (MC; a), the right and left mediolateral cavities (MLC; b), and the right and left lateral cavities (LC; c). We divided the upper mantle cavity into four cavities: the right and left interlamellar cavities of the inner demibranch (ILCID; d), and the right and left interlamellar cavities of the outer demibranch (ILCOD; e). The dorsal parts of the interlamellar cavities are usually called the epibranchial cavity. However, we did not find any anatomical structure discriminating the interlamellar cavity from the epibranchial cavity. Thus, in this study, the epibranchial cavity was included in the interlamellar cavity. In some mussels, as shown in Fig. 1A,C, the ventral ends of the right and left ID were attached to each other, and the median cavity was apparently separated into dorsal and ventral median cavities. In the mussel fixed with paraformaldehyde, the interlamellar cavities were narrow (Fig. 1A), but in the living mussels, the interlamellar cavities were filled and expanded by seawater (Fig. 1C). The interlamellar connection (IC) might be important as support for the structure of the demibranch against the pressure of the interlamellar cavities. As shown in the horizontal images (Fig. 1B,D), the OD and ID pairs were parallel and extended the whole length of the mussel. The interlamellar cavities were unified into one cavity at the posterior end of the demibranches that ran on the ventral side of the posterior adductor muscle and then connected to the exhalant siphon.

Water flow in the mussel

A typical example of the inflow effect of T_1-weighted MRI (T_{1w}-MRI) is shown in Fig. 2. While resting with closed shells, and without

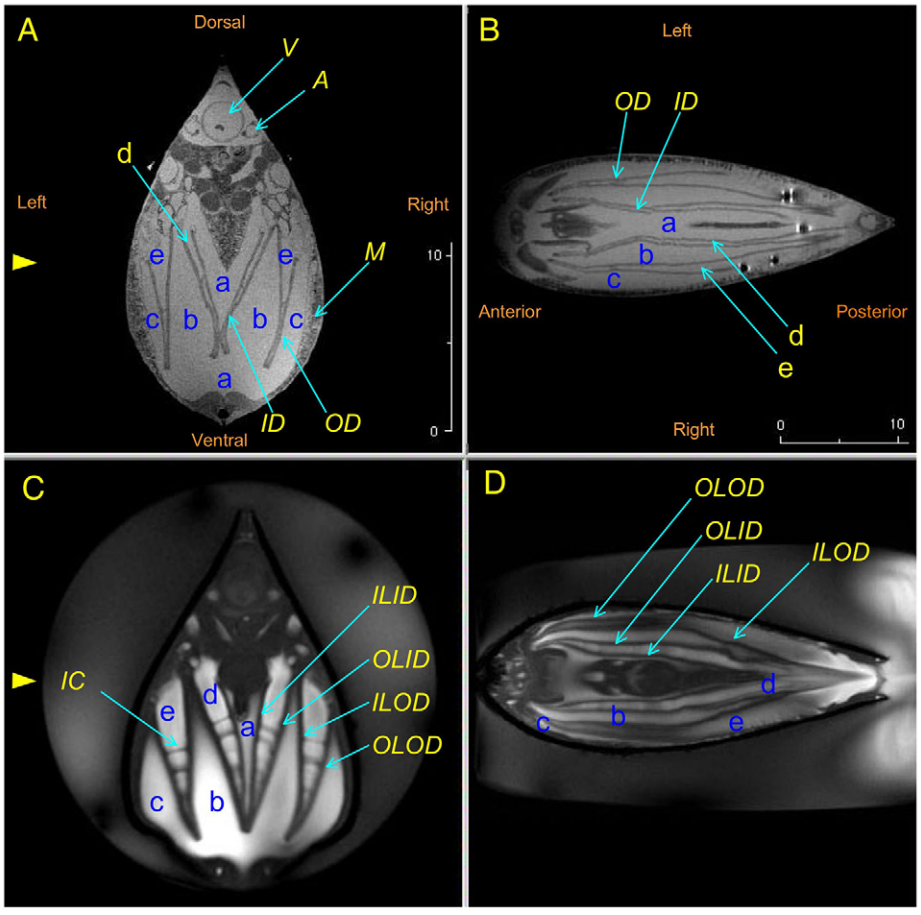

Fig. 1. Anatomical structure of the mantle cavity of *Mytilus galloprovincialis*. (A) Transverse T_2-weighted rapid acquisition with relaxation enhancement MR images of *M. galloprovincialis* fixed by paraformaldehyde at 1 mm posterior from the auriculoventricular (AV) valves. The arrowhead shows the slice position of B. (B) Horizontal image at the ventral side of the posterior adductor muscle and parallel to the long axis of the heart. (C) Transverse T_{1w}-MR images of living *M. galloprovincialis* at 1 mm posterior from the AV valves. The arrowhead shows the slice position of D. (D) Horizontal image. Labelled features: (a) median cavity (MC), (b) mediolateral cavity (MLC), (c) lateral cavity (LC), (d) interlamellar cavity of inner demibranch (ILCID), (e) interlamellar cavity of the outer demibranch (ILCOD), (ID) inner demibranch, (OD) outer demibranch, (ILID) inner lamella of the inner demibranch, (OLID) outer lamella of the inner demibranch, (ILOD) inner lamella of the outer demibranch, (OLOD) outer lamella of the outer demibranch, (IC) interlamellar connection, (V) ventricle, (A) auricle and (M) mantle. Scale bars, 10 mm.

The Journal of Experimental Biology (2014) doi:10.1242/jeb.101949

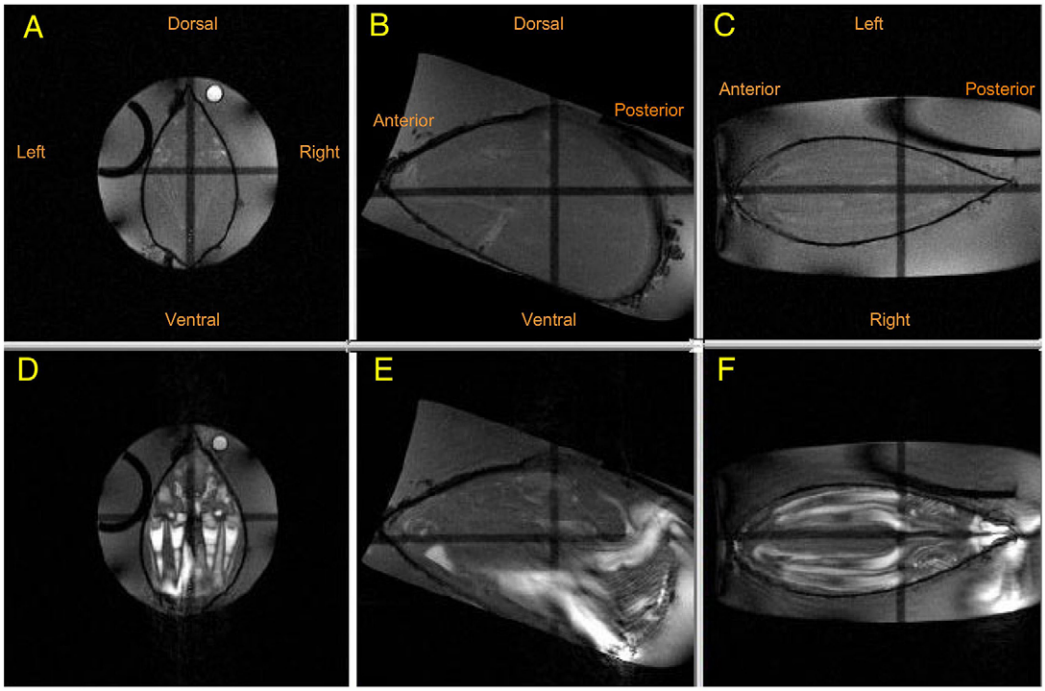

Fig. 2. T_{1w}-MR images of living *M. galloprovincialis*. Images showing the resting closed shell status (A–C), and the active open shell status (D–F) at the transverse (A,D), mid-longitudinal (B,E) and horizontal (C,F) sections. See also supplementary material Movie 1.

ventilation flow (Fig. 2A–C), the image intensity of the seawater in the mussels was almost uniform. When the mussel became active, water flow appeared in the mantle cavity, and then the image changed dramatically (Fig. 2D–F). The inflow of water perpendicular to the slice plane was depicted as a higher signal intensity. Because the water moved at a higher velocity, it was depicted as a higher signal intensity, and, as expected, the flow in the interlamellar cavities in the upper mantle cavity moved at a higher velocity than that in the lower mantle cavity (Fig. 2D,F). Water outside of the mussel was also depicted as a higher signal intensity, which might have been water to and from siphon apertures. A movie composed of transverse and horizontal images obtained every 2.55 min is presented as supplementary data (supplementary material Movie 1). As we expected, the area of the left ILCOD was 2.9±0.30 mm^2 (mean ± s.e.m., n=8) during resting status, and was expanded and kept a constant level (12.0±0.26 mm^2, n=8) during the active condition.

The flow rate and direction of seawater in living *M. galloprovincialis* were detected by phase-contrast gradient-echo MRI (PC-MRI). The anterior and posterior water flows in the mantle cavity and siphon apertures are summarized in Fig. 3. When a pair of velocity encoding gradients was applied in the anterior–posterior direction (perpendicular to the image plane), water at rest yielded no signal, and water moving within the velocity range corresponding to the velocity encoding gradient was detected. The varying flow velocities were color-coded and then overlaid with anatomical T_{1w}-MR images. Water flows in the inhalant aperture and the lower mantle cavity were laminar flows, and they were directed in the anterior direction. The velocities of the water flows in the inhalant aperture and the lower mantle cavity were 40–20 and 10–20 mm s^{-1}, respectively. The water flows in the upper mantle cavity and the exhalant siphon were also laminar flows, directed in the posterior direction. In the exhalant siphon, the average flow rate was ~40 mm s^{-1}, and peak flow rates were more than 50 mm s^{-1}. At the anterior side of the mussel (Fig. 3A), flow in the median cavity turned to the posterior direction, and the posterior flow returned through the dorsal part of the median cavity between the inner demibranches (arrowhead in Fig. 3B).

The three-dimensional flow direction and flow rate of the seawater in *M. galloprovincialis* are shown in Fig. 4. Transverse images (Fig. 4D,G,J) show that water in the lower mantle cavity flows not only in the anterior direction, but also in the dorsal–lateral direction. In the mediolateral cavity (MLC), water near the demibranches moved only in the dorsal direction. Water in the ventral part of the interlamellar cavities (ILCID and ILCOD) was directed not only in the posterior direction, but also in the dorsal direction. These results confirm that water passed through the demibranch from the lower mantle cavity to the upper mantle cavity via the interfilamentar spaces. Flow in the dorsal side of the upper mantle cavity was directed in the posterior direction, and also in the ventral and medial directions, as the upper mantle cavity tilted down to the ventral side in order to pass underneath the posterior adductor muscle (PAM) (Fig. 4E,H). In the horizontal image (Fig. 4F,I,L), water in the right and left MLCs was directed in the anterior direction. Water in the ILCID and ILCOD showed a strong flow in the posterior direction, and the flow rate increased at the posterior side of the mussel. Four water streams in the interlamellar cavities unified underneath the PAM (Fig. 4F), and the flow rate increased to a maximum (Fig. 4E). The mid-longitudinal image shows that water inflow to the inhalant aperture approached from the ventral–posterior direction. However, water outflow from the exhalant siphon was directed in the dorsal–posterior direction (Fig. 4E,H). We did not detect any flow in the PAM area at a velocity higher than 3 mm s^{-1}. All of the results are summarized in schematic diagrams of the water flow in the mantle cavity (Fig. 4M,N).

All of the mussels ejected water through the exhalant siphon. Almost all of the mussels showed water uptake through the inhalant aperture. However, two out of the 16 mussels studied spontaneously took up water via an opening on the ventral side of the mantles to the lower mantle cavity (Fig. 5).

Changes in water flow in the mussel

In order to detect abrupt changes in the water flows within a few seconds, flow images were obtained using low flip angle T_{1w}-MRI. In artificial seawater at 23°C, *M. galloprovincialis* opened their

The Journal of Experimental Biology (2014) doi:10.1242/jeb.101949

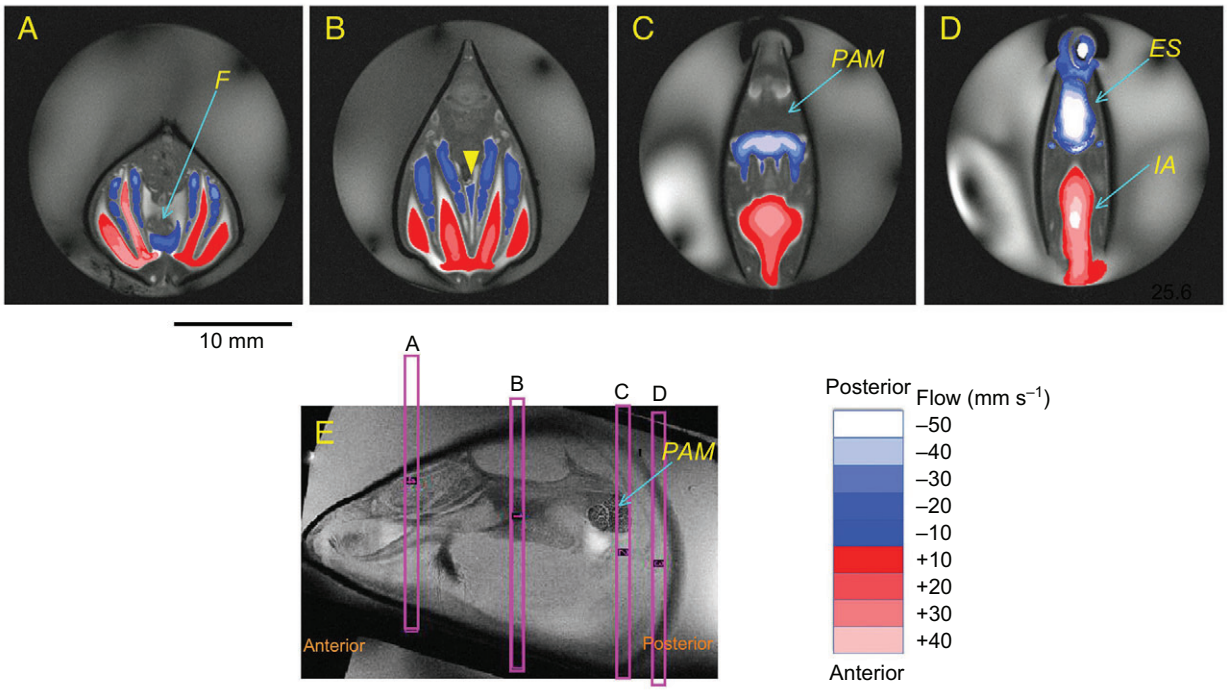

Fig. 3. Anterior–posterior flow in living *M. galloprovincialis* detected by phase-contrast MRI. (A) Transverse image of the anterior side of the mussel (8 mm anterior from the AV valve). The foot (F) appeared in the median mantle cavity. (B) Transverse image at 1 mm posterior from the AV valve. (C) Transverse image at the posterior side of the posterior adductor muscle (PAM). Four interlamellar cavities unified underneath the PAM. (D) Transverse image at the posterior end of the mussel. The inhalant aperture (IA) and exhalant siphon (ES) appear in this slice. (E) The slice positions for A to D are shown in pink boxes. Anterior- and posterior-directed flows of water are shown in red and blue, respectively.

shells and started exchanging water. Then, the mussels shut their shells and stopped the water exchange. Throughout our study, we could not detect any periodic pattern for the opening or closure of the shells, and the duration of the opening and closure cycle appeared to be random. A typical image obtained by the low flip angle T_{1w}-MRI with a higher spatial resolution is shown in Fig. 6. Changes in transverse cross-sectional area of water flow in the mantle cavity were detected every 12.8 s. When the shells closed, water flow slowed down quickly (Fig. 6B,C). When the shells opened, water flow area increased rapidly within 1 min. It is likely that water in the interlamellar cavities in the upper mantle cavity moved first (Fig. 6E), then water in the lower mantle cavity followed thereafter (Fig. 6F).

In order to detect more rapid changes in the flows in the inhalant aperture, the lower mantle cavity, the upper mantle cavity and the exhalant siphon, low flip angle T_{1w}-MR images were obtained every 1.92 s. Two slices of images, one for siphon apertures and the other for mantle cavities, were obtained at virtually the same timing, and 128 sets of images were obtained during a single measurement session for 246 s. The activity of the flows obtained from nine mussels is summarized in Table 1. In half of the 81 sessions, the mussels kept their shells open, and water flow was detected during the session (all open). The flows in the inhalant aperture, the lower mantle cavity, the upper mantle cavity and the exhalant siphon showed minimum fluctuation, and the flow was almost constant. Furthermore, we could not detect any cyclic motion of the mantle or gills (supplementary material Movie 2). The mussels did not open their shells in 5% of the sessions (all close). Mussels spontaneously opened or closed their shells during 45% of the sessions.

A typical example of the opening process of the shells is shown in Fig. 7. As shown in Fig. 7B, an increase of the area of flow in the exhalant siphon followed that of the inhalant aperture with minimal delay. In four mussels, the flow area of the exhalant siphon reached the plateau level at 30–60 s after opening their shells (0 s). Flow in the right ILCOD increased at 3 s and flow in the left ILCID also increased 1 s before the opening of the shells (Fig. 7C; supplementary material Movie 3). Therefore, flow in the exhalant siphon increased 1 s before the increase of the flow in the inhalant aperture (Fig. 7C; supplementary material Movie 3). The increase in the flow in the lower mantle cavity appeared last, because the volume is much bigger there compared with the other spaces.

In some cases, rapid oscillatory changes in water flow were detected during the opening or the closing of the shells. As shown in Fig. 8B,C and supplementary material Movie 4, flows in the inhalant and exhalant siphon apertures, and the upper and lower mantle cavities, changed within seconds. Changes in the area of the flow in the inhalant aperture were highly correlated with those in the exhalant siphon (Fig. 8D). The flow in the upper mantle cavity (total area of ILCID and ILCOD) also showed a moderate correlation with that of the inhalant aperture (Fig. 8E). However, the flow in the right ILCOD showed a low correlation with that in the inhalant aperture (Fig. 8F). The flow in the right and left ILCOD also showed independent changes (Fig. 8G).

A short closure process is shown in Fig. 9. First, flow decreased gradually, and then all of the flow stopped spontaneously at −10 s before the mussels started to close their shells. Then, the shells closed slowly from −9 to −1 s (Fig. 9B,C; supplementary material Movie 5). There was flow in the inhalant aperture in the period from −9 to −1 s, but as there were no other flows, this water flow might be a backflow from the lower mantle cavity to the inhalant aperture due to the closing of the shells. At −3 s, water flow in the upper mantle cavity increased before the opening of the shells. Then, water flows in the exhalant siphon and inhalant aperture increased with minimal delay (Fig. 9B,C).

The Journal of Experimental Biology (2014) doi:10.1242/jeb.101949

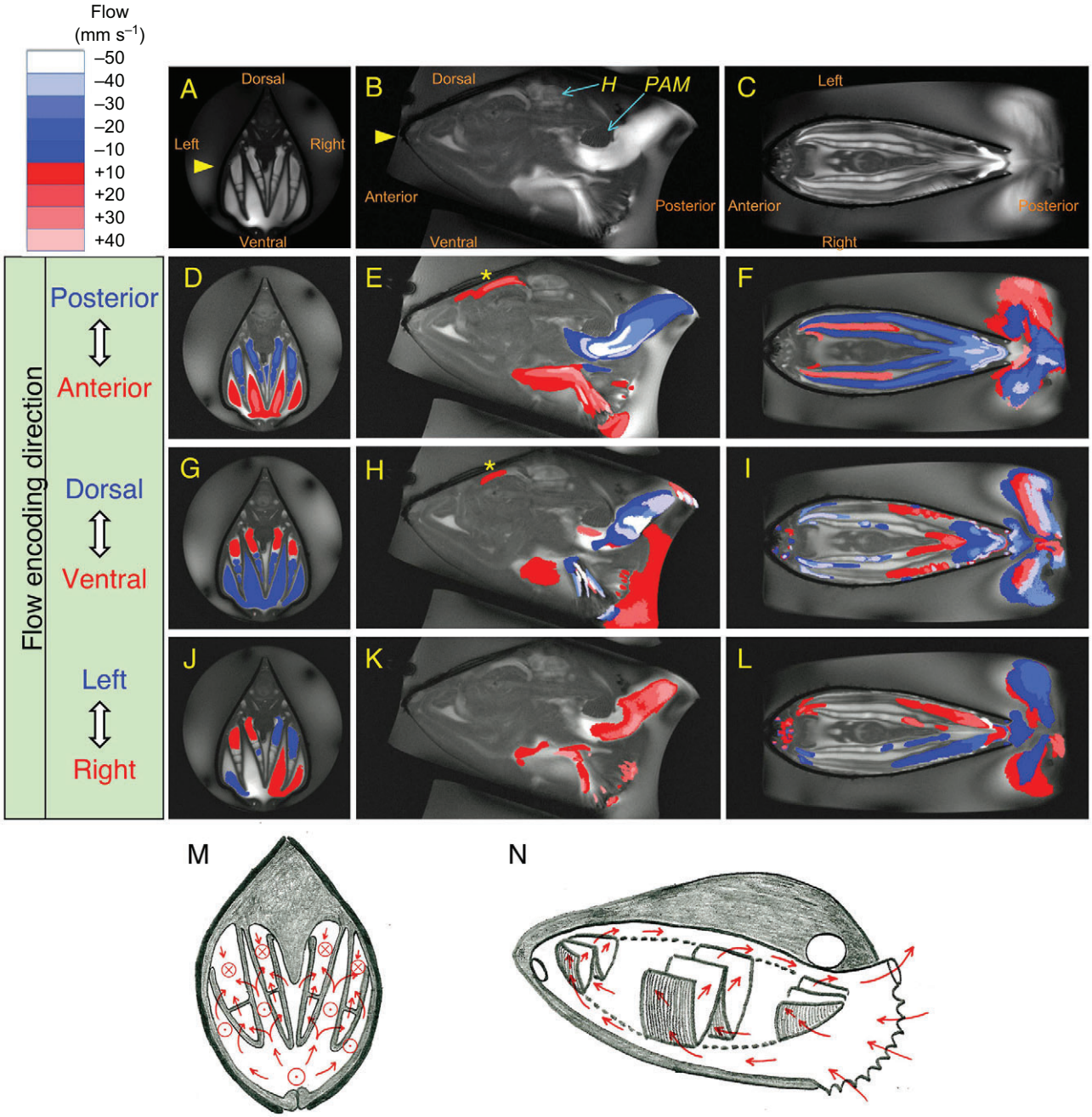

Fig. 4. Three-dimensional velocity profile of seawater in living *M. galloprovincialis*. (A) Transverse anatomical image at 1 mm posterior to the AV valve. (B) Mid-longitudinal anatomical image. H, heart. (C) Horizontal anatomical image underneath the PAM. The arrowheads in A and B represent the slice position of C. (D–F) Anterior–posterior direction of the water flow detected by phase-contrast MRI. (G–I) Ventral–dorsal direction of the water flow. (J–L) Right–left direction of the water flow. In the mid-longitudinal image (K), only the water flow to the right direction is displayed. (M,N) Schematic diagrams of water flow in the mantle cavity. The transverse view (M) shows the area 1 mm posterior to the AV valve. The longitudinal view (N) shows the left inner and outer demibranches. The direction of the water stream is shown by red arrows. Anterior- and posterior-directed flows of water are shown by ⊙ and ⊗, respectively. Asterisks in E and H show the haemolymph flow in the anterior aorta from the heart.

DISCUSSION

Flow patterns inside the shell

Wallengren (Wallengren, 1905) estimated flow in the lower mantle cavity of *Mytilus edulis* from movement of fine particles of carmine observed through a wide opening of the shells. He also surgically removed one of shells of *Mya arenaria*, and estimated water flow in the mantle cavity by observation of carmine particles through the thin and transparent mantle lobe. Since then, these techniques have been used to conduct *in vivo* observation of water flow and particle filtration in the gill (Dral, 1967; Jørgensen, 1974; Jørgensen and Ockelmann, 1991). The introduction of the video endoscopy technique (Ward et al., 1991) made it possible to observe flow not only in the lower mantle cavity, but also in the upper mantle cavity (Tankersley and Dimock, 1993). However, the ridged shaft of the optical fibre limited movement within the mantle cavity, so it is difficult to observe flow in deeper spaces, such as the dorsal parts of the lateral mantle cavity (Tankersley and Dimock, 1993). Riisgård and Larsen (Riisgård and Larsen, 2000)

The Journal of Experimental Biology (2014) doi:10.1242/jeb.101949

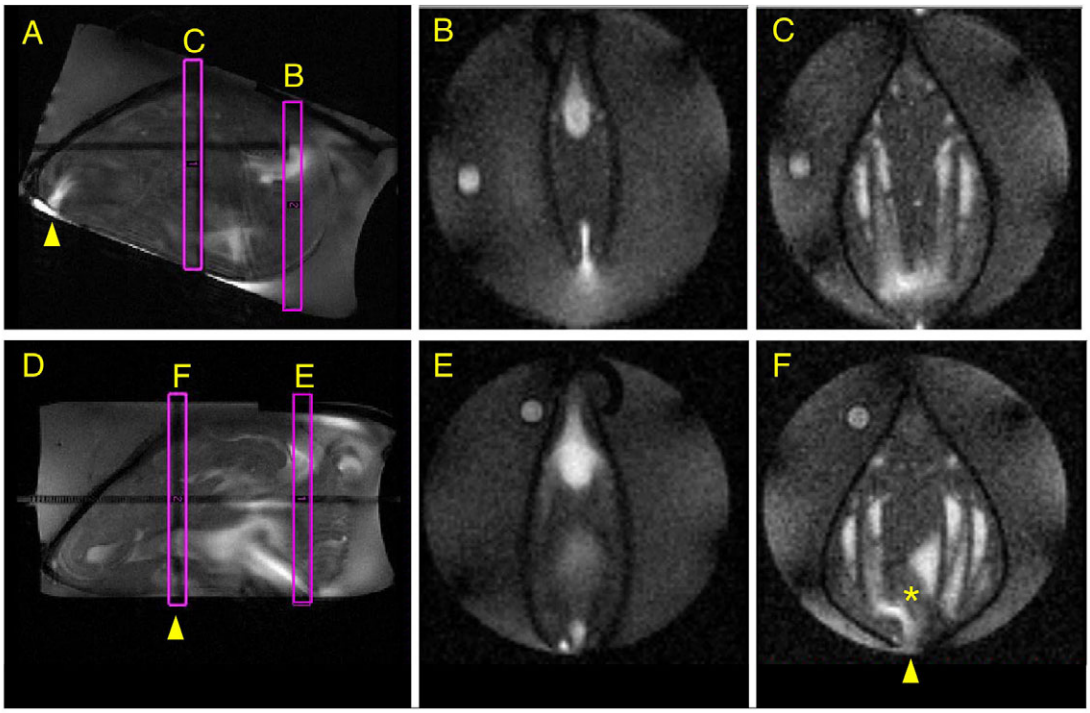

Fig. 5. T_{1w}-MR images of *M. galloprovincialis* taking up water via an opening at the ventral side of the mantles to the lower mantle cavity. One mussel (A–C) took seawater from the anterior end of the ventral side (arrowhead in A). The other mussel (D–F) took seawater from the mid ventral side (arrowheads in D and F) near the byssus filaments (* in F). In both mussels, seawater was also taken from the inhalant aperture (B,E). The slice positions of B, C, E and F are shown in pink boxes labelled B, C, E and F, respectively.

used a horizontal dissecting microscope to observe the gills of undisturbed, actively feeding *M. edulis*. The dissecting microscope is advantageous because of its wider field of view and higher magnification compared with the endoscopy technique. Furthermore, the dissecting microscope can even be employed *in vivo* in *in vitro* experiments using isolated gill filaments. The high

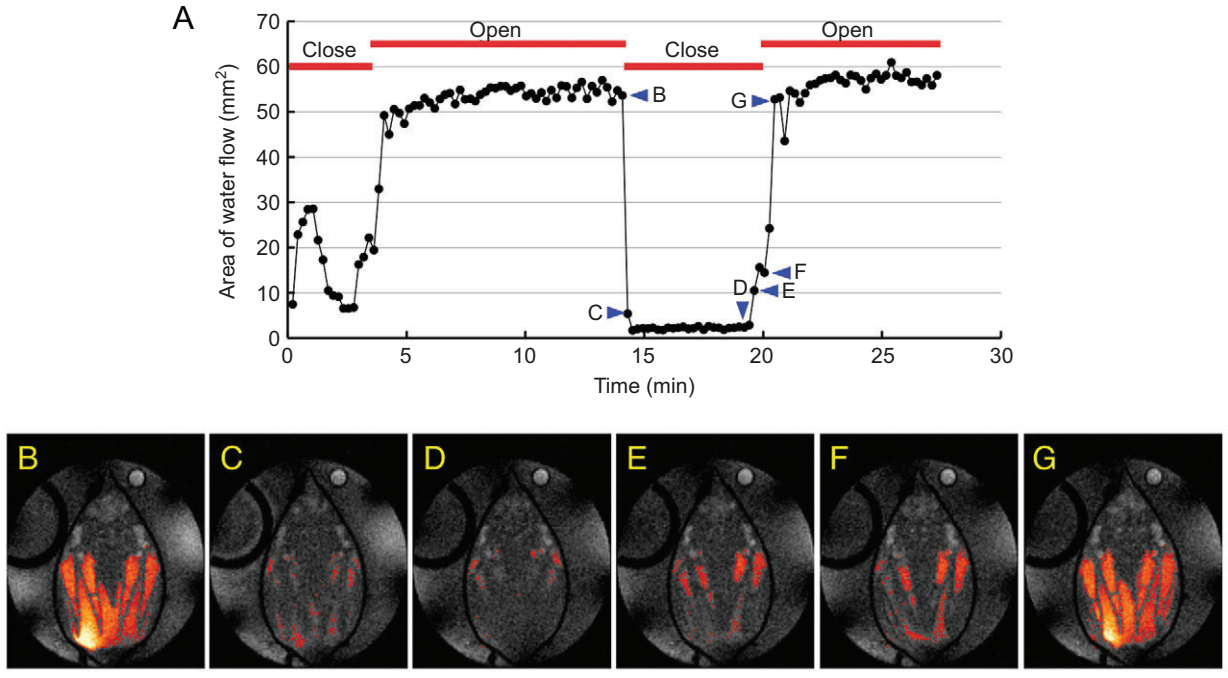

Fig. 6. Changes in water flow in the mantle cavity of *M. galloprovincialis*. (A) Changes in the transverse cross-sectional area of the water flow 1 mm posterior to the AV valve measured by a low flip angle T_{1w}-MR image every 12.8 s. The combination of relaxation delay (T_R)/echo time (T_E)/flip angle was 50 ms/3 ms/16 deg. 'Close' and 'Open' represent the closure and opening of the shell of the mussel, respectively. (B,C) Changes in the water flow before and after closure of the shells. (D–G) Changes in the water flow before and after the mussels opened their shells. The timing of each image is shown by the arrowheads labeled B to G in A. The orange pixels represent water flow.

The Journal of Experimental Biology (2014) doi:10.1242/jeb.101949

Table 1. Flow activities of *Mytilus galloprovincialis* at 23°C

Status	Number of sessions (%)	Number of mussels
Multiple open/close	9 (11.1)	4
Single close/open	15 (18.5)	6
Open to close	10 (12.3)	5
Close to open	2 (2.5)	1
All open	41 (50.6)	8
All close	4 (4.9)	3

Duration of a single measurement session was 246 s. Total number of mussels=9; total number of sessions=81. Status features: 'multiple open/close', mussels opened and closed their shells more than 2 times during one session; 'single close/open', in the beginning of the session, mussels opened their shells, spontaneously closed their shells, then opened them again during the session; 'open to close', in the beginning of the session, mussels opened their shells, then spontaneously closed their shells until the end of the session; 'close to open', in the beginning of the session, mussels closed their shells, then spontaneously opened their shells until the end of the session; 'all open', mussels kept their shells open during the session; 'all close', mussels kept their shell closed during the session.

spatial resolution of the dissecting microscope allows for the observation of the particle capture process of a single gill filament (Riisgård and Larsen, 2000). Compared with these two techniques, the spatial resolution of MRI is poor (200–100 µm), but the MRI technique we employed produced images of all of the cavities in the mussel, even when the shells were closed. The PC-MRI detected water flow without the addition of any dyes or particles. In general, the water flow inside the shell of the *M. galloprovincialis* as shown by the MRI was in agreement with that proposed by Wallengren (Wallengren, 1905) (Fig. 4M,N). When the mussel ventilated at a constant rate, the water approached the mussel from the posterior ventral side, and entered through the inhalant aperture at a flow rate of 40–20 mm s^{-1}. Then the water entered the lower mantle cavity, filled in the lower mantle cavity, and the flow rate decreased to 10–20 mm s^{-1}. The water in the lower mantle cavity flowed in the anterior dorsal direction, and passed through the interfilamentar space in the lamellae of the demibranches to the upper mantle cavity, and stretched the interlamellar cavity. In the interlamellar cavity, the flow turned in the posterior dorsal direction. The water then entered the epibranchial cavity, and the flow rate increased to approximately 20 mm s^{-1}. Then, the flows came together at the ventral side of the PAM. The average flow velocity increased to 40 mm s^{-1} in the exhalant siphon, and the flow was exhaled out in the posterior dorsal direction. Based on the cross-sectional area of the flow in the exhalant siphon (10 mm^2), the volume flow rate was estimated as 400 mm^3 s^{-1} (1.4 l h^{-1}). When *M. edulis* is stimulated by algal cells, the mussel remains fully open and exploits the filtration potential. The maximum flow rate has been estimated as 2.8 l h^{-1} for the shell length of 33.5 mm at 11.6°C (Riisgård et al., 2011). Another study (Yamamoto et al., 2013) showed that the maximum flow rates for *M. galloprovincialis* were almost constant when they were acclimatized at 15, 20 and 24°C. In the present study, the mussels were not stimulated by algal cells, and there were geometric constraints imposed by the MRI equipment. Therefore, the flow rate of the mussels shown in this study was approximately half of that shown for stimulated mussels (Riisgård et al., 2011). The flow rate shown in the lower mantle cavity was similar to that reported by Jørgensen (Jørgensen, 1981) and Famme and Kofoed (Famme and Kofoed, 1983) in *M. edulis*. The flow velocity in the exhalant siphon has been reported to be in the range of 80–30 mm s^{-1} for *Mytilus* (Maire et al., 2007; MacDonald et al., 2009; Riisgård et al., 2011). Therefore, the flow velocities observed in the other cavities in the present study might be reliable as values for an intact non-stimulated *Mytilus*.

The water in the lower mantle cavity approached the demibranches and also left from the demibranches to the interlamellar cavities at a velocity of 5–10 mm s^{-1}. Because we could not detect any signal inside the demibranches, the flow rate might be slower than 5 mm s^{-1}. Based on the volume flow rate

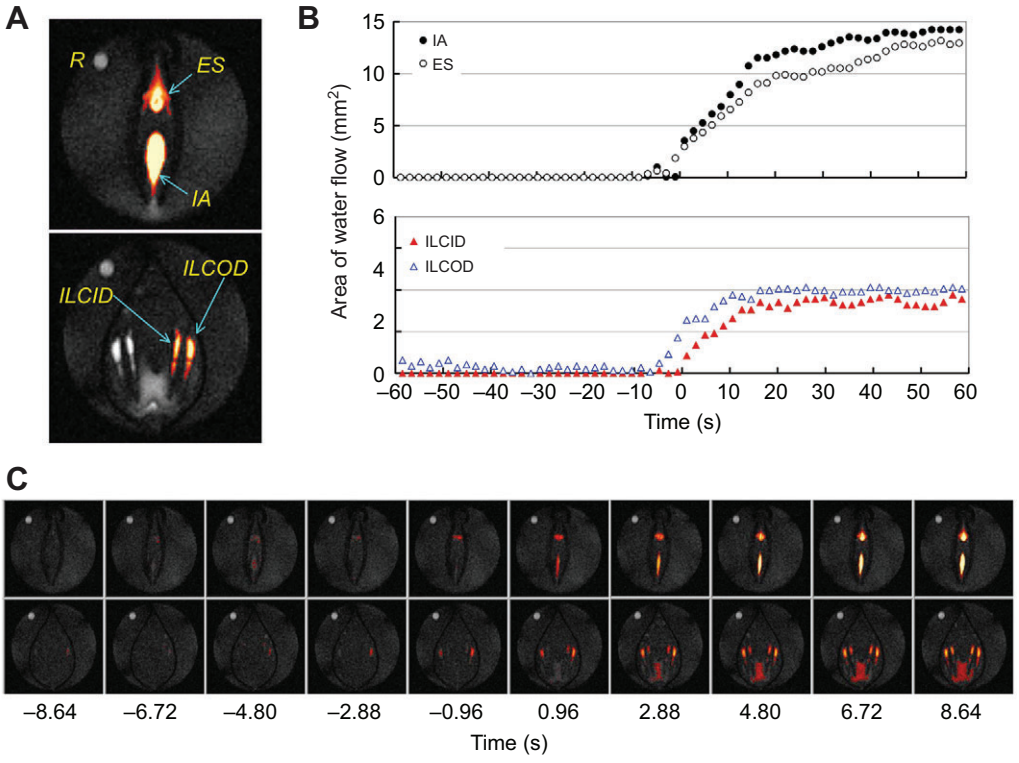

Fig. 7. Opening process of the shells of *M. galloprovincialis*. (A) Positions of the region of interest (ROI) for the inhalant aperture (IA), the exhalant siphon (ES), the right ILCOD, the right ILCID and reference (R). The orange pixels represent water flow. (B) Changes in the area of the ROIs for the IA, ES, ILCOD and ILCID. Shells opened at 0 s. (C) A series of low flip angle T_{1w}-MR images before and after the opening of the shells. See also supplementary material Movie 3.

The Journal of Experimental Biology (2014) doi:10.1242/jeb.101949

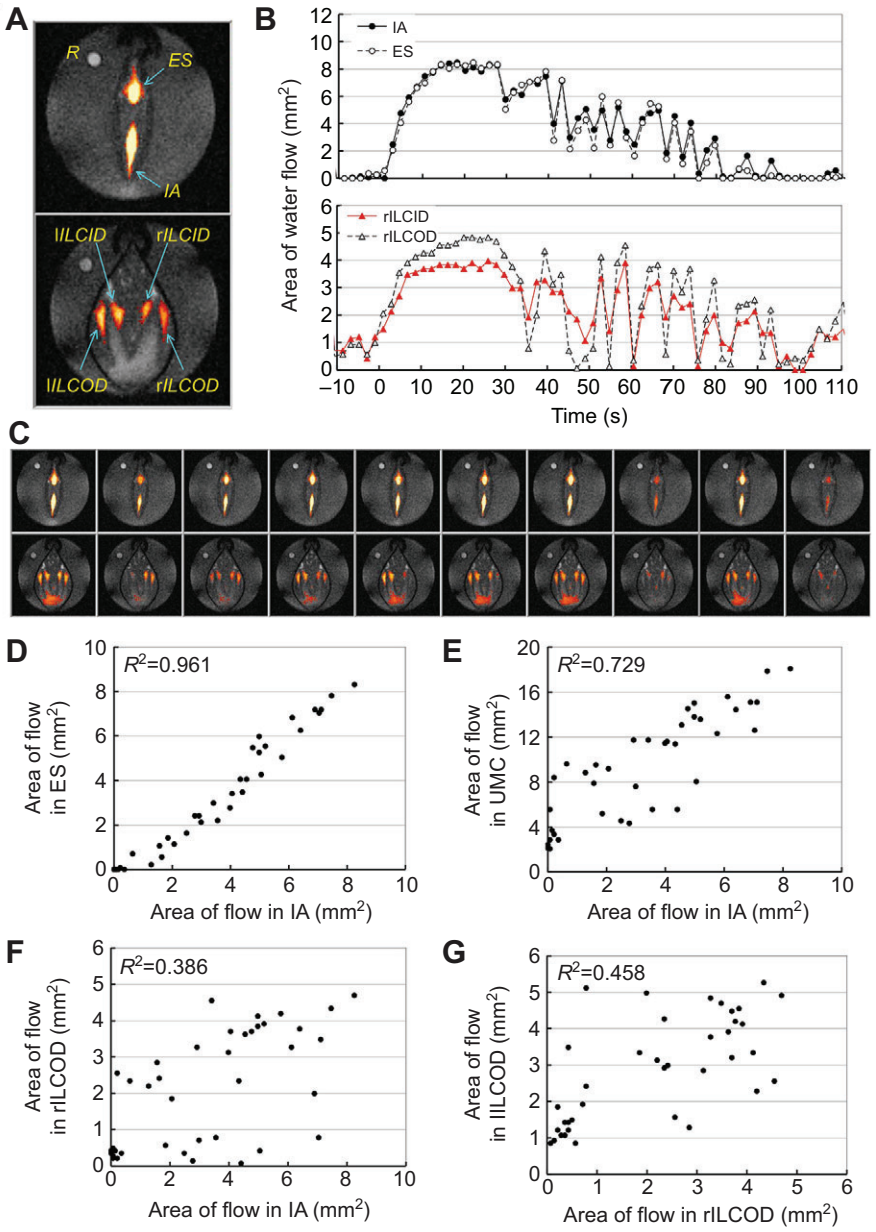

Fig. 8. Rapid changes in water flow during a slow closing process of *M. galloprovincialis*. (A) Positions of ROIs for the inhalant aperture (IA), the exhalant siphon (ES), the right and left ILCOD (rILCOD, lILCOD) and the right and left ILCID (rILCID, lILCOD). (B) Changes in the area of ROIs for the IA, ES, rILCOD and rILCID. Shells opened at 0 s. (C) A series of low flip angle T_{1w}-MR images from 27.84 to 45.12 s after the mussels opened their shells. The orange pixels represent water flow. (D–G) Correlations of the area of flow from 27.84 to 100.8 s. (D) Correlation of the area of the flow in the IA versus that in the ES. (E) Correlation of the area of flow in the IA versus the total area of flow in the upper mantle cavity (UMC) calculated from the total area of the right and left ILCOD and ILCID. (F) Correlation of the area of flow in the IA versus that in the rILCOD. (F) Correlation of the area of flow in the rILCOD versus that in the lILCOD. R^2 is the coefficient of determination (n=39). See also supplementary material Movie 4.

(F=400 mm^3 s^{-1}) in the exhalant siphon and the estimated area of gill (G=1350 mm^2) for a shell length of 33.5 mm (Riisgård et al., 2011), the flow rate in the interfilamentar canals could be estimated as $2F/G$=0.6 mm s^{-1} (Riisgård and Larsen, 2000). As we expected, this estimated value is much slower than 5 mm s^{-1}, and is approximately one-third of the values (1.41–1.7 mm s^{-1}) reported for mussels stimulated by algal cells (Riisgård and Larsen, 2000).

Even though the lateral cilia are believed to drive water flow passing through the filaments, because of a narrow interfilamentar distance, hydromechanical analysis has concluded that only small amounts of water pass between the ciliated lamella (Jørgensen, 1981). Therefore, a shunt water flow in the lower mantle cavity has been proposed. In that model, the water enters from the inhalant aperture and moves in the anterior direction via the mediolateral cavity; the flow then turns in the posterior direction via the median cavity and leaves from the exhalant siphon (Famme and Kofoed, 1983). Indeed, the presence of a posterior flow in the median mantle cavity has been discussed for more than a century (Wallengren, 1905). However, in the present study, it was clear that anterior-directed water flow was dominant in the lower mantle cavity, including the median, mediolateral and lateral cavities (Figs 3, 4). We only detected posterior-directed flow in the median cavity in the anterior side of the mussel (Fig. 3A), and the area of that flow decreased in the middle in the mussel (yellow arrowhead in Fig. 3B), and then disappeared in the posterior end of the mussel (Fig. 3C). Therefore, the reversed flow in the dorsal side of the median cavity should pass through the lamella to the upper mantle cavity. In *Mytilus*, the ends of the demibranches remain free from the mantle wall (Fig. 1A). Therefore, the presence of a shunt flow from the lateral cavity to the upper mantle cavity was assumed (Wallengren, 1905). However, as shown in Fig. 2A,D, the area of the interlamellar cavities was increased ~3-fold by the water flow, and the ends of the demibranches were attached to the mantle wall (Fig. 1C). We did not detect any direct flow from the lateral cavities to the upper mantle cavity through the free ends of the demibranches (Fig. 4G). Judging from these results, all of the water that entered from the inhalant aperture could be passed through the interfilamentar spaces of the demibranches.

The Journal of Experimental Biology (2014) doi:10.1242/jeb.101949

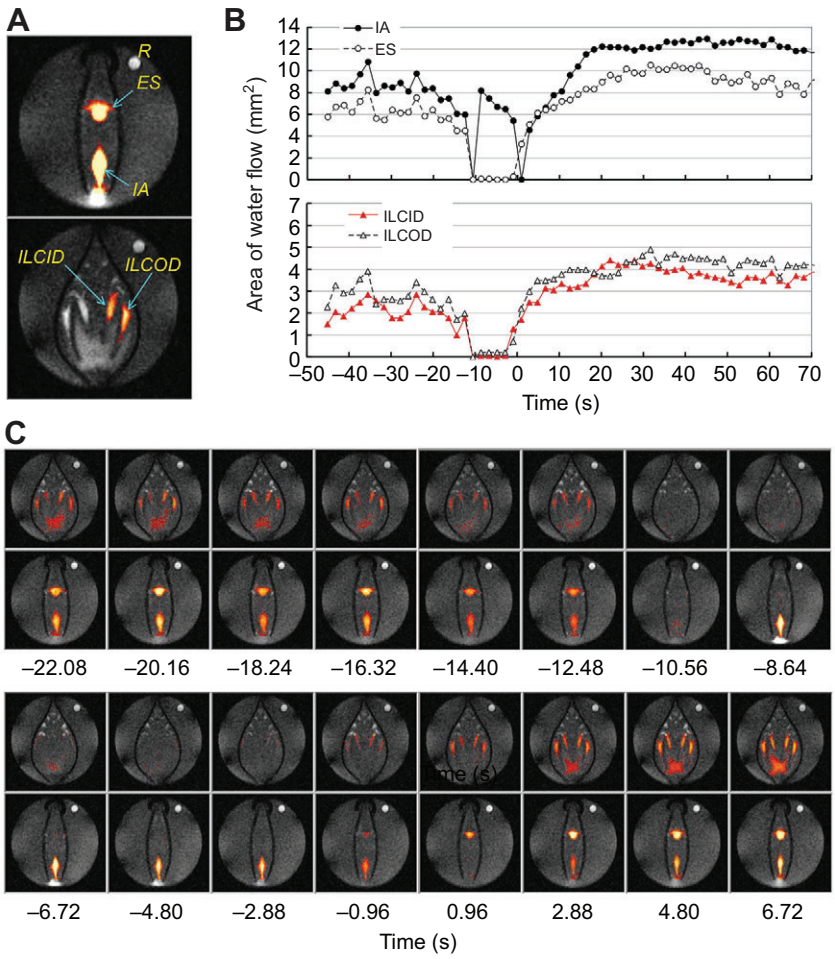

Fig. 9. A short closure process of the shells of *M. galloprovincialis*. (A) Positions of the ROI of the inhalant aperture (IA), the exhalant siphon (ES), the right ILCOD, the right ILCID and reference (R). The orange pixels represent water flow. (B) Changes in area of the ROIs for the IA, ES, ILCOD and ILCID. The shells closed and opened at approximately 0 s. (C) A series of low flip angle T_{1w}-MR images before and after the mussels opened their shells. See also supplementary material Movie 5.

Start and stop of water flow in the mussel

In the filibranchs and eulamellibranchs, it is believed that the lateral cilia are solely responsible for driving water over the demibranch and aid in production of the respiratory currents (Mill, 1972). As far as we observed, with a time resolution up to 1.92 s, the area of the anterior–posterior flow in the mantle cavity was almost constant, and we could not detect any cyclic motion of the mantle or the gill during the time period when the shells opened (supplementary material Movie 2). We also measured IntraGate MR images (retrospectively self-gated fast low angle shot sequences) (Bishop et al., 2006; Seo et al., 2014), but we could not detect any motion synchronized with the heart beat (data not shown).

In the opening process of the shells, water flow in the interlamellar cavities increased before the opening (Figs 7–9), followed by increase in the flows in the exhalant siphon and the inhalant aperture. This is direct evidence of the lateral cilia as the primary driver of water flow in the mussel. In the closed shells, a spontaneous increase in water flow was detected in the interlamellar cavities. In other words, mussels can control ciliary activity at will. Dral (Dral, 1967) reported that the *M. edulis*, in dense suspensions, can vary cilliary activity and control water flow in parts of the gills. The branchial nerve is distributed in the gill, and it was assumed that it controls the ciliary activity (Bayne, 1976).

Usually, the closure of the shells and the slow down of the water flow occurred at almost the same timing. However, in some cases, flow in the mantle cavity stopped before the closing the shells (Fig. 9). This is very impressive, because not only the flow in the interlamellar cavities, but also flows in the exhalant siphon and the lower mantle cavity, stopped at the same timing. These findings suggested that flow resistance in the interfilamentar spaces is high when beating of the lateral cilia is stopped. Unfortunately, we could not determine that flow direction by T_{1w}-MRI. The flow in the exhalant siphon during the closing of the shells (−9 to −1 s in Fig. 9C) might be backflow from the lower mantle cavity to the inhalant aperture as a result of the decrease of the volume of the lower mantle cavity.

Rapid oscillatory changes in water flow would be useful phenomena for a hydromechanical analysis of water flow in the mussel. Considering the dimension of the mantle cavity and the velocities of the water flows, it may take 2–3 s for the water to move from the inhalant aperture to the exhalant siphon. However, there was a high correlation between the area in the inhalant aperture and that in the exhalant siphon. This could be explained by the ridged shell wall, which maintains a constant volume inside the shell; alternatively, the area of either the inhalant aperture or exhalant siphon could limit the amount of the flow. On the contrary, the flow in the interlamellar cavity showed a low correlation with that in the inhalant aperture. The flow in the right and left interlamellar cavities changed independently (Fig. 8F,G). These results suggest that the mussel prefers to control the amount of flow by changing the area and region of active lateral cilia in the demibranches, and not to change the activity of the cilia, for example the beating rate, in whole demibranches.

In conclusion, a combination of PC-MRI and the inflow effect of T_{1w}-MRI allowed us to perform quantitative flow analysis in all of

The Journal of Experimental Biology (2014) doi:10.1242/jeb.101949

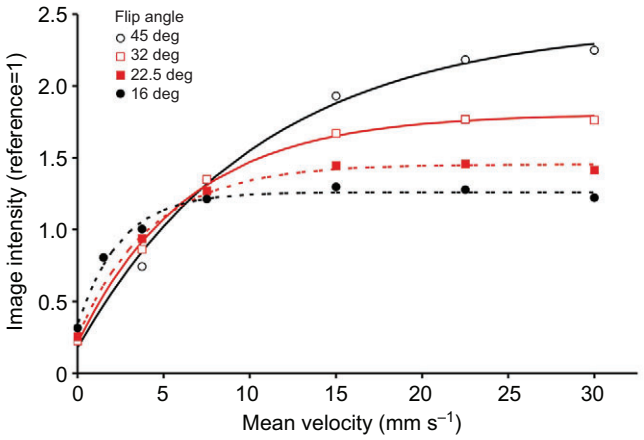

Fig. 10. Flip angle dependency of the relationship between flow velocity and image intensity. The image intensity of the seawater in a constant flow of T_{1w}-MRI obtained by a slice thickness of 2 mm with a combination of T_R/T_E=20 ms/3 ms. The image intensity was quantified compared with the image intensity of a reference containing 0.5 mmol l^{-1} $MnCl_2$ solution. The mean flow velocity of the water in the tubing was measured by phase-contrast MRI. The regression lines are the results of the function $I=a[1–\exp(–bV)]+c$, where I and V are the image intensity and velocity of the flow (mm s^{-1}), respectively, and a, b and c are constants. a and b depend on the flip angle and slice thickness, and b depends on T_1 and $1/T_R$. The results of non-linear fitting using Igor Pro 4.09A (WaveMetrics, OR, USA) were a combination of $a/b/c$=2.252±0.113/0.0943±0.0133/0.176±0.075 for a flip angle of 45 deg, 1.598±0.052/0.1565±0.0131/0.207±0.044 for a flip angle of 32 deg, 1.204±0.036/0.2381±0.0174/0.250±0.031 for a flip angle of 22.5 deg and 0.928±0.051/0.4036±0.0542/0.332±0.046 for a flip angle of 16 deg (coefficient ± s.d.).

the cavities in the mussel. Because the PC-MRI required 10 min for data acquisition, we plan to conduct further studies to estimate flow velocity from the image intensity of T_{1w}-MRI (Fig. 10). Obtaining data on the area and the velocity of flow during rapid oscillatory changes in flow would be very useful for a hydromechanical analysis of water flow in the mussel.

MATERIALS AND METHODS

Experimental mussels

Mytilus galloprovincialis were supplied by Hamasui Co., Ltd (Hatsukaichi, Hiroshima, Japan). These mussels were cultivated using a floating suspended culture bed in the Onoseto Sea off the shore of Miyajima, Hiroshima Prefecture, and collected from the culture bed on 30 October 2012 and 31 March 2013. After collection, the mussels were immersed in natural seawater, cooled by ice, and then transported to the laboratory by a refrigerated transport service, maintained at 10°C, within a time period of 16 h (Cool Ta-Q-BIN, Yamato Transport Co., Ltd, Tokyo, Japan). At the laboratory, a small number of mussels (approximately 10) were kept in aerated synthetic seawater (4 l) in a 5 l bath at room temperature (20–24°C). The synthetic seawater (salinity 3.6%) was made by dissolving a synthetic seawater mixture supplied by Matsuda Inc. (Daito, Osaka, Japan) in distilled water. Half of the volume of the seawater was exchanged every week. Mussels were fed with *Chaetoceros calcitrans* (WDB Environmental & Biological Research Institute, Kaifu, Tokushima, Japan), and 2.5×10^6 cells l^{-1} seawater in the bath were applied at intervals of 1–2 days. The experiments were conducted from 1 to 18 weeks after sampling. A total of 16 mussels were used in this study. The length, height and width of mussels were 33.5±0.35, 20.8±0.26 and 12.2±0.32 mm (means and s.e.m.), respectively. All of the animal experiments conducted in this study were carried out under the rules and regulations of the ‘Guiding Principles for the Care and Use of Animals’, as approved by the Council of the Physiological Society of Japan.

Magnetic resonance imaging

The MRI examination of *M. galloprovincialis* in this study used procedures noted in a previous report (Seo et al., 2014). In brief, the mussels were placed in a plastic tube (inner diameter of 22.5 mm), and each mussel was positioned in place using an elastic silicone strip, which was inserted at the hinge position of the shell. The mussels were immersed in 12 ml of synthetic seawater without aeration, and the temperature was kept at 23°C. The ^{1}H MR images were obtained by a 7 T microimaging system (AVANCE III, Bruker Biospin, Ettlingen, Baden-Württemberg, Germany) with ParaVison operating software (version 5.1) and equipped with an active shielded gradient (micro2.5) and a 25-mm ^{1}H birdcage radiofrequency coil. The typical imaging parameters used for the *in vivo* T_1-weighted gradient-echo MR imaging (T_{1w}-MRI) were as follows: 24×24 mm field of view with a pixel size of 94×94 µm and a slice thickness of 1 mm, 150 ms relaxation delay (T_R), 4 ms echo time (T_E), four accumulations, and a total image acquisition time of 2 min 34 s. A sinc-shaped pulse (duration 2 ms, flip angle 45 deg) was used for excitation.

The definitions of the orientation of the planes were also those employed in our previous report (Seo et al., 2014). The longitudinal plane was defined as being parallel to the plane defined by the free edges of the bivalves and the hinge. The horizontal plane was defined as being perpendicular to the longitudinal plane and parallel to the basal line of the pericardium. The transverse plane was defined as being perpendicular to the longitudinal and horizontal planes. For convenience, the slice position of the transverse image was measured from the position of the auriculoventricular (AV) valve.

Water flow

The water flow in the mussel was imaged by the inflow effect of T_{1w}-MRI (Bock et al., 2001; Seo et al., 2014). The typical imaging parameters for the high time resolution imaging used were as follows: a transverse slice with a pixel resolution of 250×250 µm and a slice thickness of 2 mm with a combination of T_R/T_E/flip angle=20 ms/3 ms/16 or 32.5 deg. Two slices of images could be obtained every 1.92 s, and the difference in the timing of the two slices was 10 ms. The inflow effect of T_{1w}-MRI was tested using a constant flow of seawater in polystyrene tubing. The velocity dependency of the image intensity is shown in Fig. 10. Using a lower flip angle (16–32.5 deg), the image intensity was almost constant at more than 15 mm s^{-1}. Therefore, a flip angle of 16 deg could be employed to detect flow, and could detect velocity down to 3 mm s^{-1}. In this study, pixels with an image intensity higher than the noise level of the static seawater were assigned as those in the flow of water. However, using a higher flip angle (45 deg), the image intensity increased when the flow velocity increased. Therefore, it might be possible to estimate flow velocity from the image intensity of the T_{1w}-MRI and the regression line shown in Fig. 10. When necessary, a higher spatial resolution image was measured with a pixel resolution of 200×200 µm and a slice thickness of 1 mm with a combination of T_R/T_E/flip angle=50 ms/3 ms/16 deg. Two slices of images could be obtained every 12.8 s, and the difference in the timing of the two slices was 25 ms.

The flow rate and direction were measured by phase-contrast gradient echo MRI (PC-MRI) (Lotz et al., 2002; Seo et al., 2014) using a transverse, longitudinal or horizontal slice with a pixel resolution of 94×94 µm and a slice thickness of 1 mm with a combination of T_R/T_E/flip angle=170 ms/5.5 ms/45 deg, two accumulations, and a total image acquisition time of 8 min 42 s. Eight pairs of velocity encoding gradients were used, with a strength corresponding to a velocity from −30 to 40 mm s^{-1} with a 10 mm s^{-1} step. Using a holding signal, the observable range of the velocity was expanded from −50 to 40 mm s^{-1}. When necessary, a lower (2–5 mm s^{-1}) and higher velocity (60–100 mm s^{-1}) could be detected using a higher or lower velocity encoding gradient, respectively.

Acknowledgements

The authors sincerely thank Dr S. Terakado (Dokkyo Medical University School of Medicine) for his translation of the old German literature. We also thank Dr T. Okutani for providing helpful comments; Drs D. Gross, V. Lehman and T. Oerther (Bruker Biospin) for their technical assistance; as well as Prof. S. Kojima (Atmosphere and Ocean Research Institute, The University of Tokyo) for his helpful suggestions and encouragement to E.S.

Competing interests
The authors declare no competing financial interests.

Author contributions
E.S., T.M. and Y.S. conceived and designed the experiments; E.S., Y.I.-O., M.M. and Y.S. performed the experiments; E.S., K.O., M.M. and Y.S. analysed the data; and E.S. and Y.S. wrote the paper. All of the authors approved the final version of the manuscript.

Funding
Parts of this study were supported by grants from the Ministry of Education, Science, and Culture of Japan (no. 24659102 to Y.S.), and the Cooperative Study Program of the National Institute for Physiological Sciences (no. 106 in 2011 and no. 145 in 2012 to Y.S., T.M. and M.M.).

Supplementary material
Supplementary material available online at
http://jeb.biologists.org/lookup/suppl/doi:10.1242/jeb.101949/-/DC1

References
Bayne, B. L. (1976). *Marine Mussels: Their Ecology and Physiology.* Cambridge: Cambridge University Press.
Beninger, P. G. and Le Pennec, M. (2006). Structure and function in Scallops. In *Scallops: Biology, Ecology and Aquaculture,* 2nd edn (ed. S. E. Shumway and J. G. J. Parsons), pp.123-227. Oxford: Elsevier Science.
Bishop, J., Feintuch, A., Bock, N. A., Nieman, B., Dazai, J., Davidson, L. and Henkelman, R. M. (2006). Retrospective gating for mouse cardiac MRI. *Magn. Reson. Med.* **55**, 472-477.
Bock, C., Frederich, M., Wittig, R.-M. and Pörtner, H.-O. (2001). Simultaneous observations of haemolymph flow and ventilation in marine spider crabs at different temperatures: a flow weighted MRI study. *Magn. Reson. Imaging* **19**, 1113-1124.
Dral, A. D. G. (1967). The movements of the latero-frontal cilia and the mechanisms of particle retention in the mussel (*Mytilus edulis* L.). *Neth. J. Sea Res.* **3**, 391-422.
Famme, P. and Kofoed, L. H. (1983). Shunt water flow throughout the mantle cavity in *Mytilus edulis* L. and its influence on particle retention. *Mar. Biol. Lett.* **4**, 207-218.
Herberholz, J., Mims, C. J., Zhang, X., Hu, X. and Edwards, D. H. (2004). Anatomy of a live invertebrate revealed by manganese-enhanced magnetic resonance imaging. *J. Exp. Biol.* **207**, 4543-4550.
Jørgensen, C. B. (1974). On gill function in the mussel *Mytilus edulis* L. *Ophelia* **13**, 187-232.
Jørgensen, C. B. (1981). A hydromechanical principle for particle retention in *Mytilus edulis* and other ciliary suspension feeders. *Mar. Biol.* **61**, 277-282.
Jørgensen, C. B. (1982). Fluid mechanics of the mussel gill: the lateral cilia. *Mar. Biol.* **70**, 275-281.
Jørgensen, C. B. and Ockelmann, K. (1991). Beat frequency of lateral cilia in intact filter feeding bivalves: effect of temperature. *Ophelia* **33**, 67-70.
Jørgensen, C. B., Møhlenberg, F. and Sten-Knudsen, O. (1986a). Nature of relation between ventilation and oxygen consumption in filter feeders. *Mar. Ecol. Prog. Ser.* **29**, 73-88.
Jørgensen, C. B., Famme, P., Kristensen, H. S., Larsen, P. S., Møhlenberg, F. and Riisgård, H. U. (1986b). The bivalve pump. *Mar. Ecol. Prog. Ser.* **34**, 69-77.
Jørgensen, C. B., Larsen, P. S., Møhlenberg, F. and Riisgård, H. U. (1988). The mussel pump: properties and modeling. *Mar. Ecol. Prog. Ser.* **45**, 205-216.
Kiørboe, T., Møhlenberg, F. and Nøhr, O. (1980). Feeding, particle selection and carbon absorption in *Mytilus edulis* in different mixtures of algae and resuspended bottom material. *Ophelia* **19**, 193-205.
Lotz, J., Meier, C., Leppert, A. and Galanski, M. (2002). Cardiovascular flow measurement with phase-contrast MR imaging: basic facts and implementation. *Radiographics* **22**, 651-671.
MacDonald, B. A., Robinson, S. M. and Barrington, K. (2009). Evaluating the use of exhalant siphon area in estimating feeding activity of blue mussels, *Mytilus edulis*. *J. Shellfish Res.* **28**, 289-297.
Maire, O., Amouroux, J. M., Duchêne, J. C. and Grémare, A. (2007). Relationship between filtration activity and food availability in the Mediterranean mussel *Mytilus galloprovincialis*. *Mar. Biol.* **152**, 1293-1307.
Mill, P. J. (1972). *Respiration in the Invertebrates*. London: Macmillan Press.
Nielsen, N. F., Larsen, P. S., Riisgård, H. U. and Jørgensen, C. B. (1993). Fluid motion and particle retention in the gill of *Mytilus edulis*: video recordings and numerical modeling. *Mar. Biol.* **116**, 61-71.
Riisgård, H. U. (2001). On measurement of filtration rate in bivalves – the stony road to reliable data: review and interpretation. *Mar. Ecol. Prog. Ser.* **211**, 275-291.
Riisgård, H. U. and Larsen, P. S. (2000). A comment on experimental techniques for studying particle capture in filter-feeding bivalves. *Limnol. Oceanogr.* **45**, 1192-1195.
Riisgård, H. U., Larsen, P. S. and Nielsen, N. F. (1996). Particle capture in the mussel *Mytilus edulis*: the role of latero-frontal cirri. *Mar. Biol.* **127**, 259-266.
Riisgård, H. U., Jørgensen, B. H., Lundgreen, K., Storti, F., Walther, J. H., Meyer, K. E. and Larsen, P. S. (2011). The exhalant jet of mussels *Mytilus edulis*. *Mar. Ecol. Prog. Ser.* **437**, 147-164.
Seo, E., Ohishi, K., Maruyama, T., Imaizumi-Ohashi, Y., Murakami, M. and Seo, Y. (2014). Testing the constant-volume hypothesis by magnetic resonance imaging of *Mytilus galloprovincialis* heart. *J. Exp. Biol.* **217**, 964-973.
Tankersley, R. A. and Dimock, R. V., Jr (1993). Endoscopic visualization of the functional morphology of the ctenidia of the unionid mussel *Pyganodon cataracta*. *Can. J. Zool.* **71**, 811-819.
Wallengren, H. (1905). *Zur Biologie der Muscheln. Zwei Bände: 1. Die Wasserströmungen. 2. Die Nahrungsaufnahme*. Lund, Sweden: Lunds Universitets Arsskrift.
Ward, J. E., Beninger, P. G., MacDonald, B. A. and Thompson, R. I. (1991). Direct observations of feeding structures and mechanisms in bivalve molluscs using endoscopic examination and video image analysis. *Mar. Biol.* **111**, 287-291.
Ward, J. E., Sanford, L. P., Newell, R. I. E. and MacDonald, B. A. (1998). A new explanation of particle capture in suspension-feeding bivalve molluscs. *Limnol. Oceanogr.* **43**, 741-752.
Yamamoto, K., Araki, A. and Handa, T. (2013). Change of ventilation in the Mediterranean blue mussel *Mytilus galloprovincialis* with feeding. *J. Natl. Fish. Univ.* **62**, 1-4.